# Journal of Materials Chemistry C

Accepted Manuscript


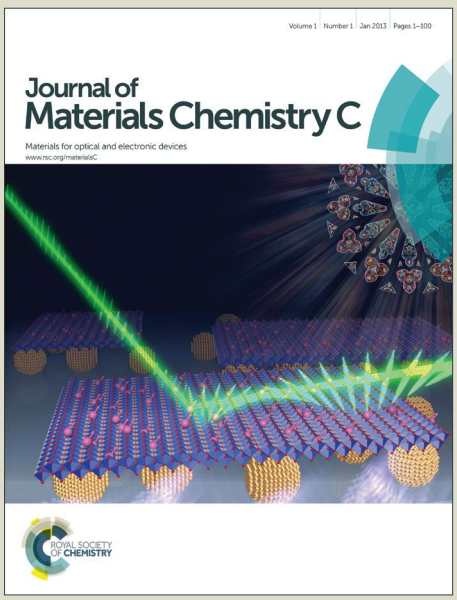





ROYAL SOCIETY OF CHEMISTRY

www.rsc.org/materialsC

# Improvements in Bending Performance and Bias Stability of Flexible InGaZnO Thin Film Transistors and Optimum Barrier Structures for Plastic Poly(ethylene naphthalate) Substrates

Min-Ji Park,[a] Da-Jeong Yun,[a] Min-Ki Ryu,[b] Jong-Heon Yang,[b] Jae-Eun Pi,[b] Oh-Sang Kwon,[b] Gi Heon Kim,[b] Chi-Sun Hwang,[b] Jun-Yong Bak,[a] Sung-Min Yoon*[a]

[a]*Department of Advanced Materials Engineering for Information & Electronics, Kyung Hee University, Yongin, Gyeonggi-do 446-701, Republic of Korea*

[b]*Electronics & Telecommunication Research Institute, Daejeon, 305-730, Republic of Korea*

**Corresponding author: sungmin@khu.ac.kr*

**Abstract**

Amorphous indium gallium zinc oxide thin-film transistors (TFTs) were fabricated and characterized on flexible Poly(ethylene naphthalate) (PEN) substrates. A hybrid inorganic/organic double-layered barrier layer structure was proposed for enhancing the permeability and surface roughness of the PEN substrates, which was composed of 3-μm-thick spin-coated organic layer and 50-nm-thick atomic-layer-deposited $Al_2O_3$ inorganic layer. The saturation mobility, subthreshold swing, and on/off ratio of the TFTs on the PEN substrates with the proposed hybrid barrier structure were obtained to be approximately 15.5 $cm^2\ V^{-1}s^{-1}$, 0.2 V/dec, and $2.2\times10^8$, respectively. These good TFT performances were not degraded even under the mechanical bending situation at a curvature radius of 3.3 mm and after the repetitive bending cycles. Furthermore, the variations in turn-on voltage of the TFT

were evaluated to be approximately as small as -0.1 and +1.6 V under the negative and positive-bias stress tests, respectively.

## 1. Introduction

Flexible electronic systems on plastic substrates have energetically been researched and developed because of their bendable, rollable, thinner, and lighter advantages.[1~2] Above all, flexible-type flat-panel displays have great potential for highly functional next-generation display applications.[3~4] Plastic substrates are most important for these applications and hence, they should be satisfied with such requirements as a low thermal expansion coefficient, a high temperature compatibility, a strong chemical stability, a high impermeability against ambient gas and moisture, and a smooth surface roughness. These properties for the plastic substrates are typically inferior to those obtained for conventional glass substrates. Consequently, the introduction of appropriate barrier structure into the plastic substrates would be an indispensable solution for flexible electronic applications, especially for improving their permeability and surface roughness.

Flexible active matrix organic light-emitting diode display panels equipped with various types of thin film transistors (TFTs) were previously demonstrated.[5~7] In particular, the TFT backplane with an amorphous In-Ga-Zn-O (a-IGZO) channel layer have actively been researched due to its high field-effect mobility and high on/off ratio even at a low process temperature, compared with conventional amorphous silicon and organic semiconductors.[8] Furthermore, the beneficial features of a-IGZO TFTs, such as excellent uniformity and robust device stability, have been suggested that they can be promising backplane devices for the flexible display panels.[9]

Generally, the polyimide (PI) has been employed for a flexible substrate owing to its high glass transition temperature ($T_g$) of around 360 $^oC$. The effect of barrier layer prepared onto the PI substrates on the device behaviors of the a-IGZO TFTs were previously investigated.[10]

However, because it significantly takes cost to use the expensive PI as a substrate for large-area electronics including the flexible displays, it would be definitely desirable to employ a cheaper plastic substrate with optimizing a process temperature for the a-IGZO TFTs under 150 $^{o}$C. The poly(ethylene naphtalate) (PEN) has features of a low $T_g$ of around 155 $^{o}$C, a low thermal expansion coefficient, and a robust chemical stability. Thus, the PEN can offer a good chance to realize flexible display panels with reasonable cost by employing the a-IGZO backplane devices at a low process temperature. Although the device characteristics of the a-IGZO TFTs fabricated on PEN substrates were previously examined,[11~13] the device behaviors are not fully optimized regarding transfer characteristics[13], mobility[12,13], bias stress stability[13], and bending performances.[11,12,13] More specifically, although the device in ref. 11 exhibited high carrier mobility of 24.3 $cm^2$/Vs and robust stability characteristics, the bending properties were not provided. The devices in ref. 12 and 13 showed relatively low carrier mobilities of 5.13 and 11.2 $cm^2$/Vs, respectively. Furthermore, the bending strain available for the device operations under the bending situations remained as just 1.5 and 0.63 %, respectively. Furthermore, the roles and functions of barrier layers introduced on the PEN substrate have rarely been investigated in previous literatures. In this work, we suggest that device performances would be enhanced by optimizing the barrier layer structures on the PEN substrate.

We fabricated a flexible a-IGZO TFTs on the PEN substrates and optimized the barrier layer structures. A hybrid organic/inorganic double-layered barrier was proposed to enhance the permeability and surface roughness of the PEN. Its superior process compatibility and barrier properties were well confirmed from two viewpoints of bending characteristics and bias stabilities of the flexible a-IGZO TFTs fabricated on the plastic PEN substrates.

## 2. Experimental Section

We fabricated a-IGZO TFTs with top-gate bottom-contact structure on the flexible poly(ethylene naphthalate) (PEN) substrates (Teonex, Teijin DuPont). The PEN substrates with the thickness of 125 μm were laminated on the glass substrates using the cool-off type adhesive (Intelimer, Nitta Corp.) for convenience of device fabrication. In order to obtain a smooth surface and a low moisture permeability, and a protection against mechanical damage, 3-μm-thick organic barrier (TR-8857-SA7, manufactured by Dongjin Semichem Co. Ltd) and 50-nm-thick inorganic $Al_2O_3$ barrier were prepared by spin-coating and atomic layer deposition (ALD), respectively. To compare the roles of each barrier layer, three-type devices were fabricated with only an organic barrier, a hybrid organic/inorganic double-layered barrier, and without any barrier, respectively. After formation of barrier layers, the 150-nm-thick indium-tin oxide (ITO) was deposited via dc sputtering and patterned by wet etching process with hydrogen-chloride-based etchant as source/drain (S/D) electrodes. After the wet etching process, we carefully performed a rinsing process with deionized water to completely remove etchant residue from the surface of device substrate. The 20-nm-thick a-IGZO channel layers with the atomic composition of 1:1:2.5 (In:Ga:Zn) were deposited by rf sputtering at room temperature. In order to prevent chemical damages during the patterning process for the active layer, the 9-nm-thick protective layer of $Al_2O_3$ was formed by ALD at 150 $^oC$.[15] Then, a 100-nm-thick $Al_2O_3$ film was deposited by ALD as a gate insulator. Contact holes were opened by removing given areas of $Al_2O_3$ by conventional photolithography and acid-based wet etching processes, in which phosphoric acid was used at a temperature of 120 $^oC$. Gate electrodes and S/D pads were formed by deposition and patterning of Al via thermal

evaporation. Post annealing processes were performed for 1 h at 180 $^{o}$C in an oxygen ambient to optimize the device characteristics. For the final step, the PEN substrates delaminated from the glass substrates by decreasing the temperature below 10 $^{o}$C.[11] The schematic cross-sectional view and optical microscopic image of the fabricated flexible a-IGZO TFT were shown in Figs. 1(a) and (b), respectively. The device characteristics including the stabilities and bending performances of the fabricated TFTs were evaluated using a semiconductor parameter analyzer (Keithley 4200SCS) in a dark box at room temperature. Channel width and length of measured TFTs were 40 and 20 μm, respectively.

**3. Results and Discussions**

The surface roughness of the substrate was one of the most critical points in guaranteeing the device behaviors including the bending performances and electrical characteristics of the IGZO TFTs prepared on flexible plastic substrates, which was supposed to be more important for the top-gate bottom-contact structure because of its back-channel effects. The surface morphologies of the PEN substrates prepared with various barrier layers were investigated by atomic force microscopy (AFM). Figures 2(a), 2(b), and 2(c) show the AFM images of the PEN without any barrier, an organic barrier, and inorganic/organic double-layered barrier on the PEN substrates, respectively. The $R_a$ values, which represent the arithmetic averages of absolute roughness values, were estimated to be 1.47 nm for the bare PEN surface. This value was found to be too high to obtain sound device behaviors. On the contrary, the $R_a$ was effectively reduced to 0.28 nm by introducing a 3-μm-thick organic barrier. After the deposition of inorganic $Al_2O_3$ barrier layer, the $R_a$ was measured to be 0.17 nm. However, this was not a significant difference in considering the relative atomic size and excellent film

conformality of ALD process. These results indicate that the PEN surfaces could be modified to be very smooth and homogeneous by the treatments with organic and inorganic barrier layers owing to the surface planarization effect of the spin-coated organic barrier with a suitable film thickness and the good conformality of the ALD-grown $Al_2O_3$ layer.[16] For conveniences, three-type devices fabricated on the PEN substrates with no barrier layer, only an organic barrier, and an inorganic/organic double-layered barrier were termed as TFT1, TFT2, and TFT3, respectively.

Figures 3(a) and 3(b) showed the drain current ($I_{DS}$)-gate voltage ($V_{GS}$) characteristics of the fabricated three flexible TFTs and corresponding device parameters calculated from each transfer characteristics, respectively. Calculated parameters were summarized in Table 2. All measurements were performed with double-sweep mode in forward and reverse directions of $V_{GS}$. While TFT1 showed a low on-current in $I_{DS}$ and a turn-on voltage ($V_{on}$) shifted in a positive direction, the TFT2 showed a higher on-current of approximately $5\times10^{-4}$ A at a $V_{GS}$ of 20 V and a $V_{on}$ at near 0 V. However, these two devices exhibited clockwise hysteretic behaviors in transfer curves, which were caused by the back-channel effect owing to the organic materials existed beneath the IGZO active channel. The proton and water molecule were captured at the surface of PEN and/or organic barrier. These results were supported by the Raman spectroscopy, as shown in Fig. 3(b). The peaks at 519, 1382, and 1631 $cm^{-1}$ corresponded to the vibration of $COO^-$ anion in carboxylic acid salt and C=C double bond structures, respectively. It reveals that hydrogen and hydronium ions might be captured at the surfaces of PEN and organic barrier layer, which was resulted in the hysteresis in $I_{DS}$ and positively shifted $V_{on}$ observed for the TFT1 and TFT2. Moreover, since the TFT1 was featured to have rough interface between the channel layer and PEN surface or gate insulator,

as confirmed by AFM, the field-effect mobility at saturation region ($\mu_{sat}$) and subthreshold swing (SS) were found to be significantly degraded. On the other hand, the introduction of hybrid double-layered inorganic/organic barrier structure could be a powerful solution to enhance the device performances. After the post annealing process, the $\mu_{sat}$, SS, threshold voltage ($V_{TH}$), and on/off ratio of the TFT3 were estimated to be approximately 15.5 $cm^2 V^{-1}s^{-1}$, 0.2 V/dec, 4.1 V, and $2.2\times10^8$, respectively. The annealing temperature of 180 $^oC$ could be considered to be lower than those for the conventional IGZO TFTs prepared on the glass substrate. The device characteristics have typically been optimized at a post annealing temperature around 300 $^oC$. However, the optimum temperature can be varied according to the IGZO composition and employed substrates.[17~20] Especially when the plastic substrates with organic barriers were employed for the flexible IGZO TFTs, the reduction of required thermal budget for the annealing process might be closely related to the effect of latent heat provided by the organic barrier or PEN substrate.[21] As results, the obtained results were superior properties to those for the previously reported oxide TFTs on the flexible substrates.[12~14]

For various flexible applications such as flexible displays and circuits, highly excellent impermeability against ambient atmospheres including $O_2$ and $H_2O$ should be guaranteed. However, it was well known that the moisture is easily transmitted through the flexible polymer substrates, and that the penetrated moisture can significantly affect the electrical characteristics of the devices. For the flexible TFTs, the permeability of the substrate was expected to have great impacts on the $V_{on}$ (or $V_{TH}$) and the current drivability. Table 1 summarized the permeability values measured for the PEN substrates with no barrier, only an organic barrier, and an inorganic/organic double-layered barrier. It was interesting to note that

the permeability of PEN substrate was not so markedly changed even when the organic barrier was treated. The permeability of PEN was just slightly improved from $1.85\times10^{-1}$ to $1.48\times10^{-1}$ g/m-day. On the contrary, the permeability was greatly enhanced to no more than $2\times10^{-3}$ g/m-day after the inorganic barrier treatment, which was actually expected to be far lower than the measured value, even though it was underestimated owing to the resolution limit of measurement apparatus. It suggested that the moisture penetration was effectively suppressed by the dense $Al_2O_3$ barrier prepared by ALD process. It would be impressive to investigate the variations in $V_{TH}$ ($\Delta V_{TH}$) and $I_{DS}$ hysteresis width ($W_{Hys}$) of the fabricated three-type devices with a lapse of shelf-test time. The $\Delta V_{TH}$ and clockwise $W_{Hys}$ for the TFT1, TFT2, and TFT3 were examined for 30 days, as shown in Figs. 4(a) and (b), respectively. While the $\Delta V_{TH}$ and $W_{Hys}$ were negligible with the time evolution for the TFT3, those for the TFT1 and TFT2 were randomly fluctuated and typically larger than those for the TFT3.

From the viewpoints of the examined moisture permeability and aging property during the shelf test, the role of $Al_2O_3$ inorganic barrier was found to be more remarkable than that of organic barrier. However, the organic barrier proved its importance for securing the bending performance. The Young's moduli of organic materials are much lower than those of conventional inorganic materials and the mechanical deformation of multi-layered structure primarily occurs on the organic layers owing to the difference in modulus of elasticity between two materials.[7] Consequently, the transfer characteristics for the TFT2 were successfully demonstrated under the bending situation with a curvature radius to 4.0 mm, in which a tensile strain was induced to the channel in parallel, as shown in Fig. 5(a). The device operations and their stability for the TFT3 were well confirmed even at a curvature radius of 3.3 mm, which corresponded to the calculated bending strain of 1.9 %, as shown in

Fig. 5(b). The device parameters of $\mu_{sat}$, $V_{TH,}$ and SS for the TFT2 and TFT3 were summarized as a function of the applied curvature radius, as shown in Figs. 5(c) and 5(d), respectively. It was also found that the transfer characteristics of the TFT2 were unstable due to the charge re-distribution during the bending test. As mentioned above, the organic barrier used in this work showed a considerable permeability and contained a large amount of proton. On the other hand, the hybridization with an ALD-grown inorganic barrier could effectively prevent the moisture penetration and proton generation and hence, the variation of device parameters under the bending test were negligible, as shown in Fig. 5(d). Therefore, the improvement in critical curvature radius, which was defined as the minimum curvature radius to be applied without a failure of device operation, for the TFT3 could be explained. For comparisons, the substrate type, process temperature, and calculated bending strain for the previously reported IGZO TFTs fabricated on plastic substrates were summarized in Table 3. Considering the substrate thickness, the flexible IGZO TFT prepared in this work exhibited good performance at the highest bending strain among the compared devices. The bending characteristics of the TFT3 were also evaluated to investigate the endurance under the repeated bending situations with tensile strain, in which the substrate was bent for 5,000 times at a curvature radius of 6.0 mm and for 10,000 times at a curvature radius of 5.0 mm. The transfer characteristics of the TFT3 did not exhibit marked changes even after the repetitive bending events, as shown in Fig. 5(e).

Negative and positive bias-stress (NBS and PBS) stabilities were also investigated for the TFT2 and TFT3, in which a $V_{GS}$ of +20 V or -20 V was continuously applied for $10^4$ s, as shown in Figs. 6(a)-6(d), respectively. Figure 6(e) plotted the $\Delta V_{TH}$'s for two TFTs as a function of stress time under the NBS and PBS tests. For the TFT2 and the TFT3, the $\Delta V_{TH}$'s

were measured to be -4.0 V/+2.2 V and -0.1 V/+1.6 V under the NBS/PBS tests, respectively. The first discussion point was positive $\Delta V_{TH}$ under the PBS test, as shown in Figs. 6(b) and 6(d). These results originated from the fact that the simple electron trapping at the interface between the gate insulator and channel layers, which was featured to show no variation in the SS, by the continuously applied $V_{GS}$ of +20 V.[22] Because the active and gate insulator layers were identically designed and fabricated for both TFT2 and TFT3, the PBS instabilities related to the interface quality were expected to be similarly observed for the two devices.

On the other hand, TFT2 and TFT3 had marked different back-channels prepared on organic and inorganic layers, respectively. The situation of back-channel for the oxide TFT could have great impacts on the NBS stabilities. For the TFT2, when the negative bias was applied for 30 s, the $V_{on}$ started to move toward 0 V. Furthermore, the $I_{DS}$ and SS were markedly enhanced. These variations were progressed as the increase in stress time and saturated at $10^4$ s. These result suggested the de-trapping events of trapped electrons and the effects of hydrogen ions for the TFT2 with IGZO/organic barrier interface at back-channel. During the initial stage of NBS test, the electrons trapped between the channel and gate insulator layers could be de-trapped and hence, the $V_{on}$ shifted in a negative direction. However, the simple electron de-trapping couldn't be responsible for the enhancement of $I_{DS}$ and SS. Two mechanisms of the plasma-induced damage and proton doping could also be feasible to explain these phenomena. When the a-IGZO channel layer was deposited on the organic layer during the sputtering process, the events of ion bombardment might induce the damages into the organic barrier and hence, the back-channel interface could be degraded. Thus, the initial SS and on/off ratio for the TFT2 was severely degraded. Because the damaged organic layer was not be fully cured at a final annealing temperature of 180 $^{o}$C, this

plasma-induced damage could be one of the origins for the fluctuated characteristics during the NBS test. Notwithstanding, the NBS stabilities were not completely explained by only the plasma effect. The time-dependent variations in device behaviors during the shelf test [Figs. 4(a) and (b)] and the NBS test [Fig. 6(a)] revealed that the gradual doping of proton could be another origin for obtained device characteristics. As confirmed from the Raman spectroscopy shown in Fig. 3(b), the undesirable protons were expected to be captured at the surface of back-channel and/or at the interface between the channel and organic barrier layers after the device fabrications. Therefore, the initial transfer characteristic exhibited unstable curve with a large SS value. When the negative bias was continuously applied during the NBS test, the protons gradually moved into the IGZO active layer as dopants by the continuous negative bias, as schematically illustrated in Fig. 6(f). Therefore, the protons were de-trapped from the organic barrier layer and back-channel interface and hence, the back-channel was cured and the interface quality was enhanced. Consequently, the $V_{on}$ negatively shifted and $I_{DS}$ and SS were simultaneously improved.[23~24] However, when most captured protons were liberated, the $V_{on}$ shift was saturated near the 0 V. As results, the TFT2 experienced a dramatic recovery with the progress of NBS by the enhanced interface quality at the back-channel and finally obtained device characteristics were comparable to those of the TFT3. However, one-day after, its enhanced characteristics were degraded again because of the back-channel deterioration caused by the high permeability and the proton diffusion. These results paradoxically reveal that the optimum structure of the barrier layer was important to guarantee the device reliabilities of the IGZO TFTs prepared onto the PEN substrates.

On the contrary, the plasma-induced damage and the proton doping effect could be

eliminated by the hybridization of inorganic barrier onto the organic barrier layer. As a result, the $\Delta V_{TH}$ of TFT3 was as small as -0.1 V under the NBS tests. These bias stability characteristics obtained for the TFT3 fabricated with a low thermal budget below than 180 $^{o}$C were far superior to those for the previously reported oxide TFTs on the flexible substrates.[10,13] Furthermore, this result was one of the best performance when compared to those for the IGZO TFTs fabricated on glass substrates.[25~27]

## 4. Conclusions

We have fabricated and characterized the a-IGZO TFTs on the flexible PEN substrates, in which the barrier layer structures were varied to investigate their effects on the device performance including the bias-stress stability and bending characteristics. Three-type TFTs were prepared on the PEN with no barrier, only an organic barrier, and a hybrid inorganic/organic double-layered barrier. The PEN substrate treated with the proposed hybrid barrier exhibited marked improvements in both surface smoothness and ambient impermeability. The hybrid barrier was composed of 3-μm-thick spin-coated SA7 organic and 50-nm-thick ALD grown $Al_2O_3$ inorganic layers. The mechanical bending performance was also found to be sufficiently desirable. From these investigations, it was evidently confirmed that the flexible IGZO TFTs prepared on PEN with the hybrid double-layered barrier layer exhibited excellent device characteristics. The $\mu_{sat}$, SS, threshold voltage ($V_{TH}$), and on/off ratio were evaluated to be approximately 15.5 $cm^2 V^{-1}s^{-1}$, 0.2 V/dec, 4.1 V, and $2.2\times10^8$, respectively. These characteristics were not markedly influenced by a mechanical stress even at a curvature radius of 3.3 mm and under the $10^4$-times repetitive bending cycles

at a curvature radius of 5.0 mm. Furthermore, favorable NBS and PBS stabilities could also be obtained thanks to the suitably designed barrier layer, even compared with those for the IGZO TFTs optimized on the glass substrates. It was concluded that the bending performance and bias stability of the flexible IGZO TFTs could be significantly improved by the introduction of a hybrid inorganic/organic double-layered barrier layer on the PEN substrates, and that this methodology would be a big help for reducing the thermal budget and fabrication cost for the TFT arrays for future flexible electronic applications.

**Acknowledgments**

This research was supported by the National Research Foundation of Korea (NRF) grant funded by the Korean government (MEST) (2014023501). This research was also funded by the MSIP (Ministry of Science, ICT & Future Planning), Korea in the ICT R&D Program (The core technology development of light and space adaptable energy-saving I/O platform for future advertising service). Authors thank Mr. P. H. Lee of Hwajin TS, Korea, and Nitta Corporation, Japan for their help in using of Intelimer adhesive.

**Reference**


1. M. Koo, K. I. Park, S. H. Lee, M. Suh, D. Y. Jeon, J. W. Choi, K. Kang and K. J. Lee, *Nano Lett.*, 2012, **12**, 4810
2. J. W. Seo, J. W. Park, K. S. Lim, S. J. Kang, Y. H. Hong, J. H. Yang, L. Fang, G. Y. Sung and H. K. Kim, *Appl. Phys. Lett.*, 2009, **95**, 133508
3. D. E. Mentley, *Proc. IEEE.*, 2002, **90**, 453
4. J. T. Smith, B. O'Brien, Y. K. Lee, E. J. Bawolek and J. B. Christen, *J. Display Technology*, 2014, **10**, 514
5. L. Zhou, A. Wanga, S.-C. Wu, J. Sun, S. Park and T. N. Jackson, *Appl. Phys. Lett.*, 2006, **88**, 083502
6. C. C. Wu, S. D. Theiss, G. Gu, M. H. Lu, J. C. Sturm, S. Wagner and S. R. Forrest, *IEEE Electron Device Lett.*, 1997, **18**, 609
7. J. K. Jeong, D. U. Jin, H. S. Shin, H. J. Lee, M. Kim, T. K. Ahn, J. Lee, Y. G. Mo and H. K. Chung, *IEEE Electron Device Lett.*, 2007, **28**, 389
8. K. Nomura, H. Ohta, A. Takagi, T. Kamiya, M. Hirano and H. Hosono, *Nature (London)*, 2004, **432**, 488
9. J.F. Wager, *Science*, 2003, **300**, 1245
10. K. C. Ok, S. H. K. Park, C. S. Hwang, H. Kim, H. S. Shin, J. Bae and J. S. Park, *Appl. Phys. Lett.*, 2014, **104**, 063508
11. S. H. Yang, J. Y. Bak, S. M. Yoon, M. K. Ryu, H. C. Oh, C. S. Hwang, G. H. Kim, S. H. Ko Park and J. Jang, *IEEE Electron Device Lett.*, 2011, **32**, 1692
12. H. C. Lai, Z. Pei, J. R. Jian and B. J. Tzeng, *Appl.Phys.Lett.*, 2014, **105**, 033510
13. H. Xu, J. Pang, M. Xu, M. Li, Y. Guo, Z. Chen, L. Wang, J. Zou, H. Tao, L. Wang and J. Peng, ECS J. Solid State Science and Technology, 2014, **3**, Q3035
14. N. Munzenrieder, G. A. Salvatore, T. Kinkeldei, L. Petti, C. Zysset, L. Buther and G. Troster, in *Proceeding of 71st Annual IEEE Device Reaserch Conference (DRC)*, 2013, p. 165
15. S. H. Ko Park, D. H. Cho, C. S. Hwang, S. H. Yang, M.K. Ryu, C.W. Byun, S. M. Yoon, W. S. Cheong, K. I. Cho and J. H. Jeon, *ETRI J.*, 2009, **31**, 653.
16. O. Sneh, B. Robert, C. Phelps, R. Ana, Londergand, J. Winkler and T.E. Seidel, *Thin*

*Solid Films*, 2002, **402**, 248

17. M. K. Ryu, S. H. K. Park, C. S. Hwang and S. M. Yoon, *Solid State Electronics*, 2013, **89**, 171.
18. J. Y. Bak and S. M. Yoon, *J. Vac. Sci. Technol. B*, 2012, **30**, 041208.
19. J. Y. Bak, S. H. Yang, M. K. Ryu, S. H. K. Park, C. S. Hwang and S. M. Yoon, *ACS Appl. Mater. Interfaces*, 2012, **4**, 5369.
20. J. Y. Bak, M. K. Ryu, S. H. K. Park, C. S. Hwang and S. M. Yoon, *IEEE Transactions on Electron Devices*, 2014, **61**, 2404.
21. M. Miyasaka, H. Hara, N. Karaki, S. Inoue, H. Kawai and S. Nebashi, *Japanese J. Appl. Phys.*, 2008, **47**, 4430
22. J. K. Jeong, H. W. Yang, J. H. Jeong, Y. G. Mo and H. D. Kim, *Appl. Phys. Lett.*, 2008, **93**, 123508
23. H. Godo, D. Kawae, S. Yoshitomi, T. Sasaki, S. Ito, H. Ohara, H. Kishida, M. Takahashi, A. Miyanaga and S. Yamazaki, *Jpn. J. Appl. Phys.*, 2010, **49**, 03CB04
24. B. D. Ahn, H. S. Shin, H. J. Kim, J. S. Park and J. K. Jeong, *Appl. Phys. Lett.*, 2008, **93**, 203506
25. J. K. Jeong, *Semicond. Sci. Thechnol.*, 2011, **26**, 034008
26. M. D. H. Chowdhury, P. Migliorato and Jin Jang, *Appl. Phys. Lett.*, 2011, **98**, 153511
27. T. C. Chen, T. C. Chang, T. Y. Hsieh, W. S. Lu, F. Y. Jian, C. T. Tsai, S. Y. Huang and C. S. Lin, *Appl. Phys. Lett.*, 2011, **99**, 022104
28. J. S. Park, T. W. Kim, D. Stryakhilev, J. S. Lee, S. G. An, Y. S. Pyo, D. B. Lee, Y. G. Mo, D. U. Jin and H. K. Chung, *Appl. Phys. Lett.*, 2009, **95**, 013503
29. J. Jang, M. H. Choi, B. S. Kim, W. G. Lee and M. J. Seok, *SID'12 Digst.*, 2012, **43**, 260

**Table captions**

**Table 1**. Permeability values of bare PEN substrate and barrier-treated PEN substrates with organic, inorganic, and organic/inorganic layers.

| Substrate | PEN | PEN+ Organic barrier | PEN+ Inorganic barrier | PEN + Organic/Inorganic barrier |
|---|---|---|---|---|
| Permeability [g/m-day] | $185 \times 10^{-3}$ | $148 \times 10^{-3}$ | $< \sim 1 \times 10^{-3}$ | $< \sim 1 \times 10^{-3}$ |

**Table 2.** Summary of device parameters such as mobility, threshold voltage, subthreshold swing, and current on/off ratio, for the TFT1, TFT2 and TFT3, respectively.

| Device | Saturation Mobility [$cm^2/Vs$] | Threshold Voltage [V] | Subthreshold Swing [V/dec] | On/Off Ratio |
|---|---|---|---|---|
| TFT 1 | 1.11 | 9.4 | 0.4 | $3.1 \times 10^7$ |
| TFT 2 | 14.4 | 2.8 | 0.4 | $1.5 \times 10^9$ |
| TFT 3 | 15.5 | 4.1 | 0.2 | $4.7 \times 10^9$ |

**Table 3.** Summary of substrate type, process temperature, and calculated bending strain values for the a-IGZO TFTs prepared on plastic substrates, including the device proposed in this work. The bending strain was calculated by the equation of [strain = thickness of substrate / (2×curvature radius)].

| Reference | Substrate | Process temperature (°C) | Substrate thickness (μm) | Bending radius (mm) | Strain (%) |
|---|---|---|---|---|---|
| 10 | Polyimide | 250 | 20 | N/A | N/A |
| 11 | PEN | 150 | 125 | N/A | N/A |
| 12 | PEN | 100 | 125 | 4 | 1.56 |
| 13 | PEN | 160 | 50 | 4 | 0.63 |
| | PEN | 160 | 125 | 10 | 0.63 |
| 14 | Polyimide | 115 | 50 | 2 | 1.25 |
| 28 | Polyimide | 350 | 10 | 3 | 0.17 |
| 29 | Polyimide | N/A | 25 | 2 | 0.63 |
| This work | PEN | 180 | 125 | 3.3 | 1.89 |

**Figure captions**

**Figure 1.** (Color online) (a) Schematic cross-sectional view and (b) microscopic photo image of the fabricated a-IGZO TFT on a flexible PEN substrate.

**Figure 2.** (Color online) AFM images of surface morphologies for the PEN substrates (a) with no barrier, (b) organic barrier, and (c) organic/inorganic double-layered barrier, respectively.

**Figure 3.** (Color online) (a) Sets of $I_{DS}$-$V_{GS}$ transfer curves for the fabricated three-type flexible TFTs with no barrier (TFT1), organic barrier (TFT2), and organic/inorganic double-layered barrier (TFT3), respectively. (b) Summary of variations in saturation mobility, threshold voltage, and S parameter for the three-type TFTs. (c) Raman spectroscopy of the PEN substrate.

**Figure 4.** (Color online) Variations in (a) threshold voltage shift and (b) clock-wise hysteresis width for the fabricated TFT1, TFT2, and TFT3 as a function of shelf-test time.

**Figure 5.** (Color online) (a) Sets of $I_{DS}$-$V_{GS}$ transfer curves and (c) variations in saturation mobility, threshold voltage and S parameter of the TFT2 as a function of applied curvature radius under the bending situations. (b) Sets of $I_{DS}$-$V_{GS}$ transfer curves and (d) variations in saturation mobility, threshold voltage and S parameter of the TFT3 as a function of curvature radius. (e) $I_{DS}$-$V_{GS}$ transfer curves for the TFT3 after 5,000 times bending events at a

curvature radius of 6 mm and after 10,000 times bending events a curvature radius of 5 mm under the cyclic bending situations.

**Figure 6.** (Color online) Variations in the $I_{DS}$-$V_{GS}$ characteristics with the evolution of stress time under the (a) NBS at $V_{GS}$ of -20 V and (b) PBS at $V_{GS}$ of +20 V for the TFT2 and under the (c) NBS at $V_{GS}$ of -20 V and (d) PBS at $V_{GS}$ of +20 V for the TFT3, respectively. All measurements were performed for $10^4$ s at room temperature. (e) Schematic illustration for the feasible NBS instability mechanism for the TFT prepared on the organic barrier. The protons ($H^+$) were incorporated from the PEN and/or organic barrier to the bulk region of channel layer.

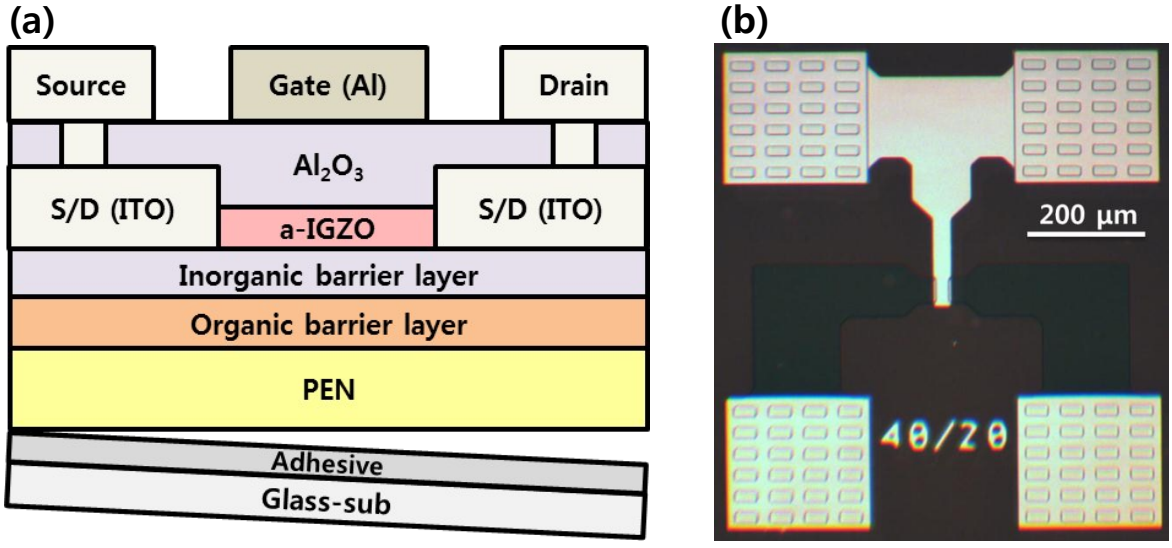

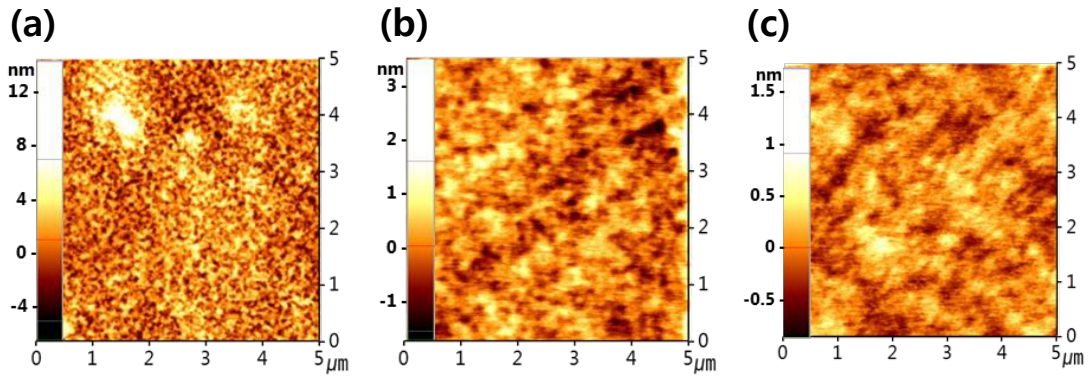

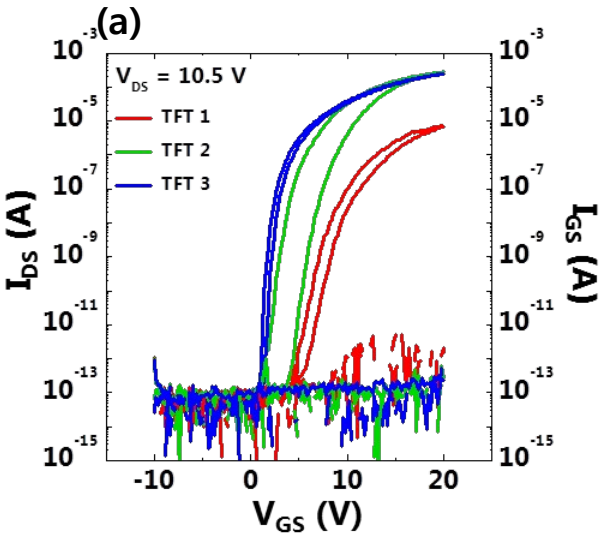


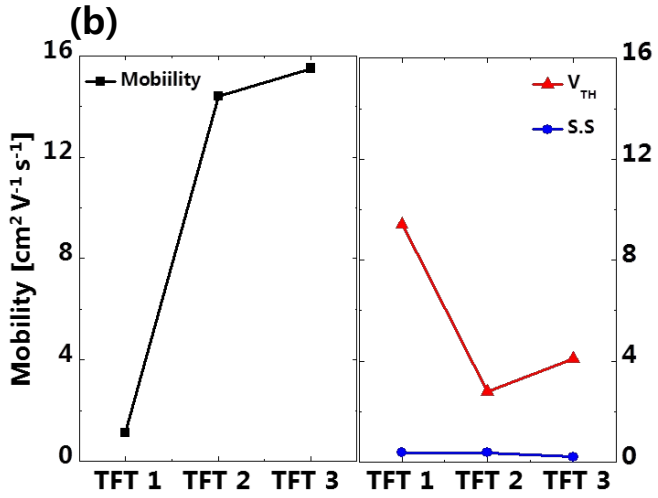


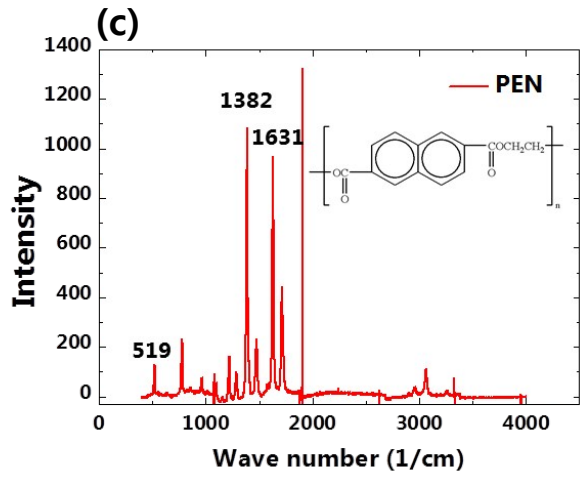

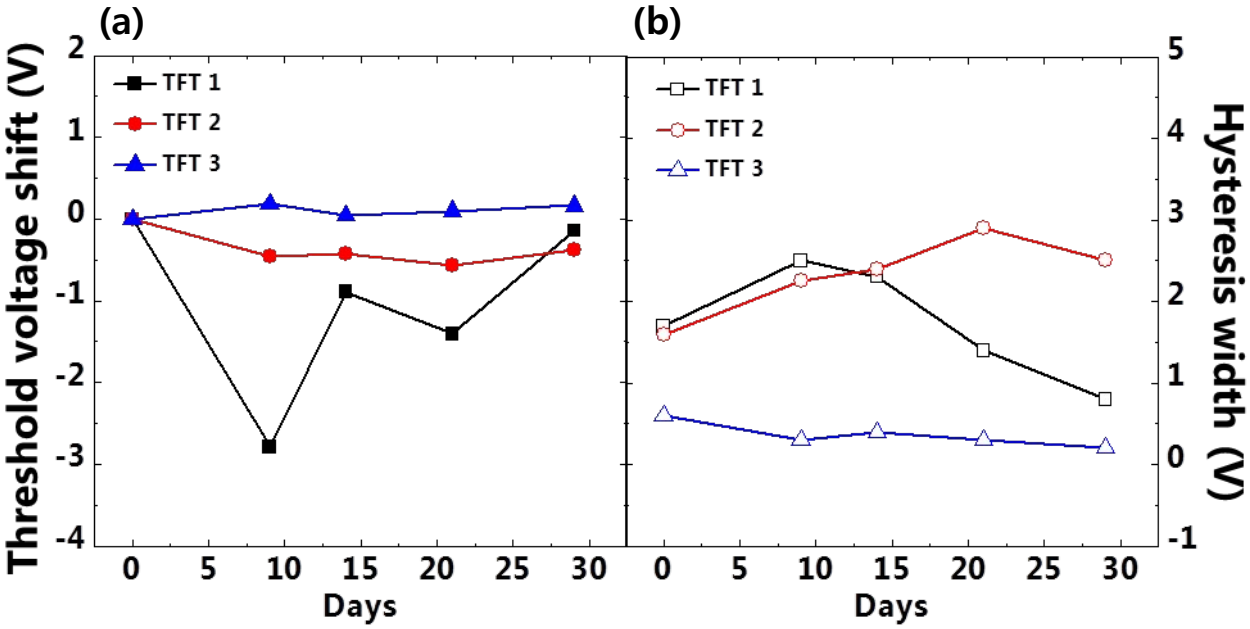

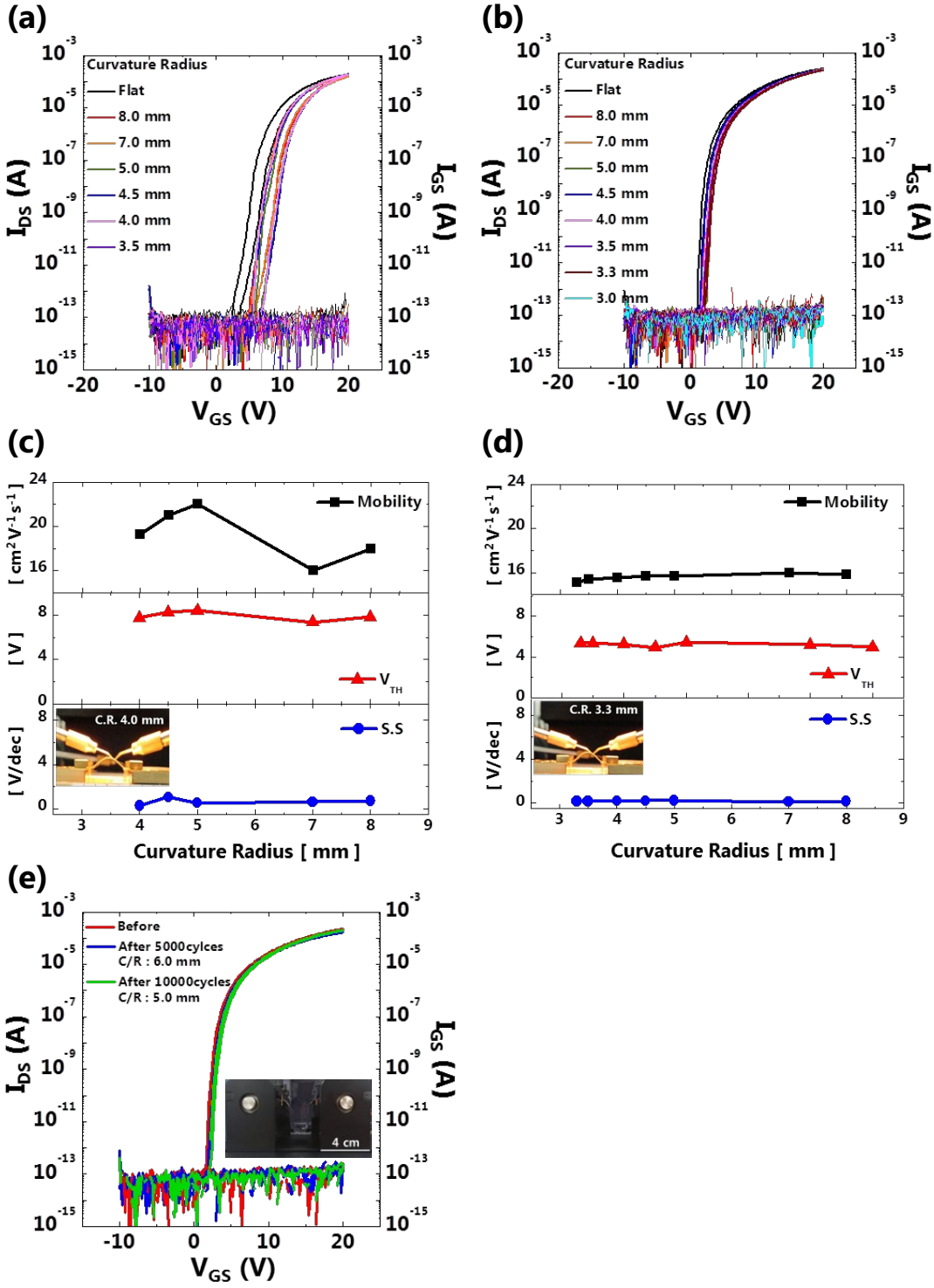

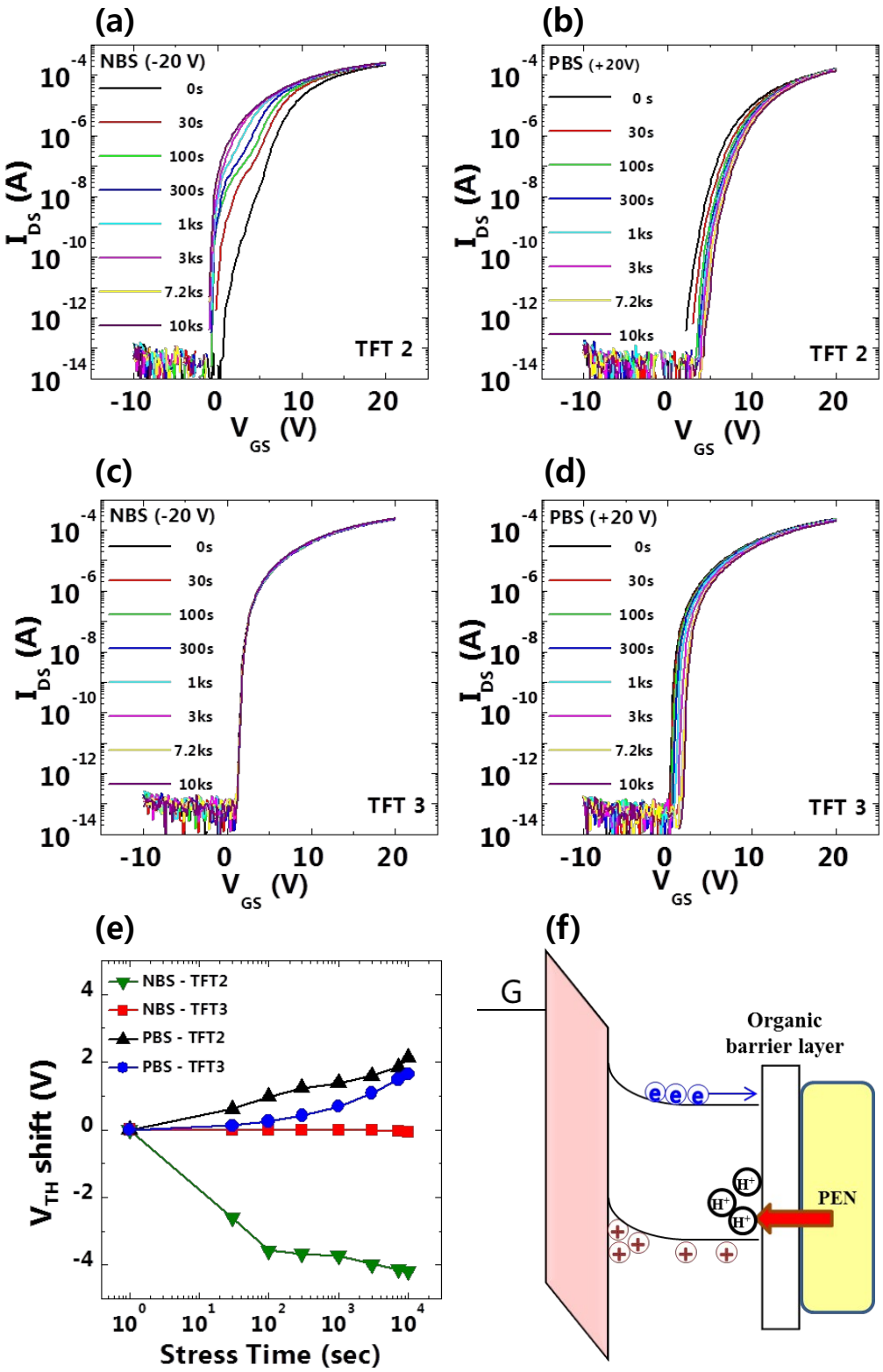

Bending characteristics of flexible oxide thin-film transistors could be enhanced by optimizing the barrier layers on the polyethylene naphthalate substrate.